

# Three-layer Flows in the Shallow Water Limit

*By Francisco de Melo Viríssimo and Paul A. Milewski*

*Dedicated to Roger Grimshaw*

---

We formulate and discuss the shallow water limit dynamics of the layered flow with three layers of immiscible fluids of different densities bounded above and below by horizontal walls. We obtain a resulting system of four equations, which may be non-local in the non-Boussinesq case. We provide a systematic way to pass to the Boussinesq limit, and then study those equations, which are first order PDEs of mixed type, more carefully. We show that in a symmetric case the solutions remain on an invariant surface and using simple waves we illustrate that this is not the case for non-symmetric cases. Reduced models consisting of systems of 2 equations are also proposed and compared to the full system.

---

## 1. Introduction

The study of internal waves in stratified fluids continues to attract much attention, as these waves are ubiquitous in the atmosphere and the ocean (see e.g. [1], [2]). They play an important role in transporting energy over long distances, and, when they break, contribute to mixing [3]. Horizontally propagating waves are usually long: their horizontal scales are much longer than the vertical ones [4]. The simplest fluid configuration for internal waves are layered interfacial flows, where the fluid is assumed to be stratified in layers of constant density. The study of these flows in the long wave limit approximates physical settings where there are sharp density variations, and yield a variety of mathematical models, depending on the relative strength of different effects. The resulting models

---

Address for correspondence: Prof. P. A. Milewski, Department of Mathematical Sciences, University of Bath, Bath, BA2 7AY, United Kingdom; email: P.A.Milewski@bath.ac.uk

can either be weakly or fully nonlinear, and dispersive or non-dispersive. Physically, nonlinearity is controlled by the wave amplitude relative to the height of the fluid domain, whereas dispersion is controlled by the relative size of horizontal length scales compared to this domain height. Strongly nonlinear, non-dispersive approximations take the form of hyperbolic or mixed type first order PDEs, first derived in this context by Long [5]. Weakly nonlinear dispersive approximations result in Korteweg-de Vries type models [6], [7] and fully nonlinear dispersive approximations lead to the so-called Miyata-Camassa-Choi system [8], [9].

In this paper we consider a strongly nonlinear non-dispersive setting in the case of three layers (and thus two interfaces) bounded above and below by horizontal walls. This case is important as it captures mode 2 internal waves - which is a slower family of waves with out-of-phase pycnocline displacements - in addition to the faster mode 1 waves. These waves, although less common than mode 1 waves have now been observed in the ocean [10]. The case of two-layer flows in the non-dispersive setting has been studied extensively (see *e.g.* [5], [11], [12]) and since the resulting equations are a system of 2 first order PDEs, certain results can be obtained analytically. For example, one can find precise conditions that ensure that the solutions remain in the hyperbolic domain up to breaking [12] or construct shock solutions in the internal dam-break (lock exchange) problem [13], [14]. The case of three layer flows is much more complicated as the resulting equations are a system of 4 PDEs and many of the methods used before no longer apply. There have been few mathematical studies of three-layer flows in the literature (see *e.g.* [15] for a three-layer Miyata-Camassa-Choi type model) and this paper aims to provide the grounds for further investigations in the subject.

We first derive the equations governing the flow in the non-Boussinesq case and show that the nature of the resulting system is dependent on the boundary conditions. For many cases the system is non-local, a result linked to the paradox of non-conservation of horizontal momentum [16]. We then turn to the dynamics in the Boussinesq limit, where we show that certain symmetric mode 2 solutions are confined to an invariant two-dimensional subspace of the four-dimensional phase plane, propose new variables that better capture mode 1 and mode 2 solutions and use simple waves to show that this invariant manifold construction is not possible for non-symmetric solutions. Finally we propose some reduced models in terms of systems of 2 PDEs that can be used to approximate the individual modes.

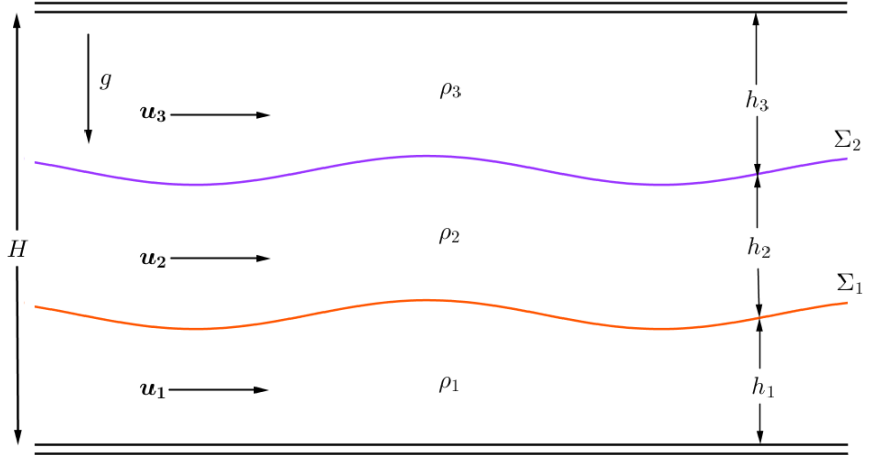


Figure 1: Schematic illustration for the three-layer problem.

## 2. Formulation

Consider a two-dimensional, irrotational flow of ideal, incompressible and immiscible fluids in three layers of different densities, under the action of gravity and bounded by horizontal rigid lids at the bottom and at the top, as shown in Figure 1.

The fluid pressure and velocity fields in each layer are given by  $p_j(x, y, t)$  and  $\mathbf{u}_j(x, y, t) = (u_j(x, y, t), v_j(x, y, t))$  respectively, with  $j = 1$  representing the lower layer,  $j = 2$  representing the middle layer and  $j = 3$  representing the upper layer. The fluid density is given by  $\rho_j$ ,  $j = 1, 2, 3$ , where the fluid in a layer is denser than the one above it, *i.e.*,  $\rho_1 \geq \rho_2 \geq \rho_3$ . The height of each of the active layers is given by  $h_j(x, t)$  and the interface between the layers, assumed to be a graph, are given by  $\Sigma_1 = \{(x, y) : y = h_1(x, t)\}$  and  $\Sigma_2 = \{(x, y) : y = (h_1 + h_2)(x, t)\}$ , as schematically indicated in the Figure 1.

The mathematical model [4], [17] for the dynamics in each layer is given by the incompressible Euler equations

$$\rho_j \frac{D\mathbf{u}_j}{Dt} = -\nabla p_j - \mathbf{F}_j, \quad (1)$$

$$\nabla \cdot \mathbf{u}_j = 0, \text{ for } j = 1, 2, 3. \quad (2)$$

for  $j = 1, 2, 3$ , with  $\mathbf{F}_j$  being the external force field. In this model, only gravitational forces act, with  $\mathbf{F}_j = (0, \rho_j g)$ .

The boundary conditions are the *impermeability conditions*, respectively given at the bottom and top walls by

$$v_1 = 0 \quad \text{on} \quad y = 0, \quad (3)$$

$$v_3 = 0 \quad \text{on} \quad y = H; \quad (4)$$

the *kinematic condition* (KBC) and the *dynamic condition* (DBC) on  $\Sigma_1$ , respectively given by

$$h_{1,t} + u_1 h_{1,x} = v_1, \quad (5)$$

$$h_{1,t} + u_2 h_{1,x} = v_2, \quad (6)$$

$$p_1 = p_2; \quad (7)$$

and the KBC and DBC on  $\Sigma_2$ , given by

$$(h_1 + h_2)_t + u_2 (h_1 + h_2)_x = v_2, \quad (8)$$

$$(h_1 + h_2)_t + u_3 (h_1 + h_2)_x = v_3, \quad (9)$$

$$p_2 = p_3. \quad (10)$$

The kinematic boundary conditions above imply, for  $j = 1, 2$ , and  $\mathbf{n}_j$  being the normal to  $\Sigma_j$ , that

$$\mathbf{n}_j \cdot \mathbf{u}_j = \mathbf{n}_j \cdot \mathbf{u}_{j+1}$$

on the interface  $\Sigma_j$ . This states the continuity of normal velocity across interfaces. The model can also be shown to satisfy

$$h_1 + h_2 + h_3 = H, \quad (11)$$

where  $H$  is the constant height of the channel, as shown in Figure 1.

### 2.1. Governing equations

Our aim is to rewrite equations (1) to (11) as a  $4 \times 4$  system of first order PDEs in the *long-wave limit* [4], [17], [18] where the vertical variation in the horizontal velocity is small, and its vertical average represents it well.

In order to proceed, we shall compute the layer average of the quantities  $u_j$ ,  $v_j$  and  $p_j$  on each layer. For instance, the vertical mean of  $u_j$ , for  $j = 1, 2, 3$ , is defined as

$$\overline{u_j}(x, t) \doteq \frac{1}{h_j(x, t)} \int_{y_j(x, t)}^{y_j(x, t) + h_j(x, t)} u_j(x, y, t) dy,$$

where  $y_j(x, t)$  is the coordinate of the lower interface of the  $j$ -th layer. Expressions for the mean of differentiated quantities are written in terms of their means. For instance, for  $u_{j,x}$ ,

$$(h_j \overline{u_j})_x = h_j \overline{u_{j,x}} + ((y_j + h_j)_x u_j|_{y=y_j+h_j} - y_{j,x} u_j|_{y=y_j}). \quad (12)$$

*2.1.1. Conservation of volume equations.* Taking the layer averages of the incompressibility condition (2) and using (12) lead to

$$(h_j \overline{u_j})_x - ((y_j + h_j)_x u_j|_{y_j+h_j} - y_{j,x} u_j|_{y_j}) + (v_j|_{y_j+h_j} - v_j|_{y_j}) = 0, \quad (13)$$

for  $j = 1, 2, 3$ . From the KBC on each interface we obtain

$$h_{j,t} + (h_j \overline{u_j})_x = 0, \quad (14)$$

which states the *conservation of volume* (or conservation of mass) for the flow in each layer.

*2.1.2. Momentum equations.* Taking the layer averages of the horizontal component of the momentum equations (1) for  $j = 1$ , using (12) for  $x$  and  $t$  derivatives and using bottom impermeability (3), we obtain

$$\begin{aligned} \rho_1 (h_1 \overline{u_1})_t + \rho_1 \left( h_1 \overline{u_1^2} \right)_x & - \rho_1 u_1|_{h_1} (h_{1,t} + u_1|_{h_1} h_{1,x} - v_1|_{h_1}) \\ & = -(h_1 \overline{p_1})_x + p_1|_{h_1} h_{1,x}. \end{aligned}$$

Here, and in what follows, we have denoted  $p$  on  $\Sigma_j$  by  $P_j$ , and the bottom and top pressures by  $P_0$  and  $P$  respectively. Applying the KBC on  $\Sigma_1$  in the expression above gives

$$\rho_1 \left( (h_1 \overline{u_1})_t + \left( h_1 \overline{u_1^2} \right)_x \right) = -(h_1 \overline{p_1})_x + P_1 h_{1,x}. \quad (15)$$

This same averaging applied to the middle layer yields

$$\rho_2 \left( (h_2 \overline{u_2})_t + \left( h_2 \overline{u_2^2} \right)_x \right) = -(h_2 \overline{p_2})_x + P_1 h_{1,x} - P_2 (h_1 + h_2)_x, \quad (16)$$

and for the upper layer,

$$\rho_3 \left( (h_3 \overline{u_3})_t + \left( h_3 \overline{u_3^2} \right)_x \right) = -(h_3 \overline{p_3})_x - P_2 (h_1 + h_2)_x. \quad (17)$$

Equations (15) to (17) are exact but are not closed, as they relate the evolutions of mean quantities to means of products. A closure is provided by the shallow water approximation.

*2.1.3. The shallow water limit.* The shallow water approximation is obtained by imposing two conditions. First, all horizontal variations are slowly-varying compared to vertical ones. This is done formally by scaling horizontal derivatives with a small parameter  $\mu$  relative to vertical derivatives. Incompressibility in each layer then imposes that  $v$  must scale with  $\mu$ . Second, we impose that vorticity is  $\mathcal{O}(\mu^2)$ , which requires  $u_{j,y} = \mathcal{O}(\mu^2)$ . This implies that the horizontal velocities are uniform in  $y$

to leading order and can be written as

$$u_j(x, y, t) = \overline{u_j}(x, t) + \mu^2 \tilde{u}_j(x, y, t). \quad (18)$$

From this we immediately concludes that

$$\overline{u_j^2} = \overline{u_j}^2 + \mu^4 \overline{\tilde{u}_j^2}. \quad (19)$$

Under these rescalings, the vertical component of the Euler equations reads as (see [12])

$$\mu^2 \rho_j (v_{j,t} + u_j v_{j,x} + v_j v_{j,y}) = -p_{j,y} - \rho_j g, \quad (20)$$

implying that the leading order pressure satisfies the hydrostatic balance

$$p_{j,y} = -g\rho_j + \mathcal{O}(\mu^2). \quad (21)$$

Integrating, and imposing continuity of pressure at each interface yields

$$p_1(x, y, t) = \rho_1 g(h_1 - y) + \rho_2 g h_2 + \rho_3 g h_3 + P, \quad (22)$$

$$p_2(x, y, t) = \rho_2 g(h_1 + h_2 - y) + \rho_3 g h_3 + P, \quad (23)$$

$$p_3(x, y, t) = \rho_3 g(H - y) + P. \quad (24)$$

With equations (19) and (22) to (24) we simplify the averaged horizontal momentum equations (also dropping the overbars and setting  $g = 1$ ) to obtain

$$\rho_1 (u_{1,t} + u_1 u_{1,x}) + (\rho_1 - \rho_3) h_{1,x} + (\rho_2 - \rho_3) h_{2,x} = -P_x, \quad (25)$$

$$\rho_2 (u_{2,t} + u_2 u_{2,x}) + (\rho_2 - \rho_3) (h_{1,x} + h_{2,x}) = -P_x, \quad (26)$$

$$\rho_3 (u_{3,t} + u_3 u_{3,x}) = -P_x. \quad (27)$$

Conservation of mass for each layer now reads

$$h_{j,t} + (h_j u_j)_x = 0. \quad (28)$$

We shall normalise the height  $H$  and the densities such that

$$h_1 + h_2 + h_3 = 1, \quad (29)$$

$$\rho_1 + \rho_2 + \rho_3 = 3. \quad (30)$$

The set (25) to (30) consists of a closed system of seven equations for the seven unknowns  $h_1, h_2, h_3, u_1, u_2, u_3, P$ . In solving for the pressure later, we will see that in most cases the equation for  $P$  has an elliptic nature with important consequences.

*2.1.4. The volume flux.* The *volume flux* is defined as

$$Q(x, t) \doteq h_1 u_1 + h_2 u_2 + h_3 u_3. \quad (31)$$

Summing the conservation of mass equations gives  $Q_x(x, t) = 0$  and hence  $Q$  is a function of  $t$  only. Its time evolution is

$$\begin{aligned}
 Q'(t) = & - \left( h_1 u_1^2 + h_2 u_2^2 + h_3 u_3^2 + \frac{h_1^2 + h_2^2}{2} \right)_x \\
 & - h_2 h_{1,x} - h_1 \left( \frac{\rho_2}{\rho_1} h_{2,x} + \frac{\rho_3}{\rho_1} h_{3,x} \right) - \frac{\rho_3}{\rho_2} h_2 h_{3,x} \\
 & - \left( \frac{h_1}{\rho_1} + \frac{h_2}{\rho_2} + \frac{h_3}{\rho_3} \right) P_x. \tag{32}
 \end{aligned}$$

This equation can be solved for *both*  $P$  and  $Q$  given boundary conditions. For example,  $Q$  may set by the boundary conditions on  $u_j$  and  $h_j$ . Two scenarios in which this occurs are in the presence of vertical sidewalls, implying  $Q = 0$ , or when far field inlet conditions fix  $Q$  to a constant value which can then be transformed away through a Gallilean transformation by choosing an appropriate reference frame in (33)–(36) below. In both cases, Equation (32) becomes immediately an equation for  $P_x$ . On the other hand, if boundary conditions for  $P$  are known, then the equation can be integrated in  $x$  and the boundary conditions applied, yielding an expression for  $Q'$ . This expression can be substituted back into (32), again yielding an equation for  $P_x$ . The details of this last case are shown in the next chapter.

*2.1.5. Reduction to smaller systems.* We shall recast the system in new variables. Introduce the *differences of layer thickness*

$$\begin{aligned}
 d_1 &= h_2 - h_1, \\
 d_2 &= h_3 - h_2,
 \end{aligned}$$

which track the displacement of interfaces, and the *shear* variables

$$\begin{aligned}
 w_1 &= u_2 - u_1, \\
 w_2 &= u_3 - u_2.
 \end{aligned}$$

These together with the identities (30) and (31) give a transformation between the variables  $(h_1, h_2, h_3, u_1, u_2, u_3)$  and the variables  $(d_1, d_2, w_1, w_2, Q)$ . The evolution depends only on these 5 variables, and we write these equations below. In what follows, we define the parameters

$$r_1 = \frac{\rho_2}{\rho_1} = 1 - r, \quad r_2 = \frac{\rho_3}{\rho_2} = 1 - rR,$$

where  $r \geq 0$ ,  $R > 0$  are positive constants (*Atwood numbers* [4]), and the following rescaled variables:

$$\begin{aligned}\tilde{w}_j &= \frac{w_j}{\sqrt{r}}, & \tilde{t} &= t\sqrt{r}, & q &= \frac{Q}{\sqrt{r}}, \\ rp &= \frac{P}{(1 + r_1 + r_1r_2)}.\end{aligned}$$

Under these changes, our equations become

$$\begin{aligned}d_{1,t} + qd_{1,x} + \left( \frac{w_1}{3}(1 - d_2) - \frac{d_1}{3}(w_1 + w_2) \right)_x \\ - \left( \frac{d_1^2}{3}(2w_1 + w_2) + \frac{d_1d_2}{3}(w_1 + 2w_2) \right)_x = 0,\end{aligned}\quad (33)$$

$$\begin{aligned}d_{2,t} + qd_{2,x} + \left( \frac{w_2}{3}(1 + d_1) + \frac{d_2}{3}(w_1 + w_2) \right)_x \\ - \left( \frac{d_2^2}{3}(w_1 + 2w_2) + \frac{d_1d_2}{3}(2w_1 + w_2) \right)_x = 0,\end{aligned}\quad (34)$$

$$\begin{aligned}w_{1,t} + qw_{1,x} + \left( \left( \frac{2d_1 + d_2}{3} \right) (1 - w_1^2) - \frac{w_1w_2}{3} (1 + d_1 + 2d_2) - \frac{w_1^2}{6} \right)_x \\ - \frac{rR}{3} \left( \frac{1 + d_1 + d_2}{3} \right)_x = rp_x,\end{aligned}\quad (35)$$

$$\begin{aligned}w_{2,t} + qw_{2,x} + \left( \left( \frac{d_1 + 2d_2}{3} \right) (R - w_2^2) + \frac{w_1w_2}{3} (1 - 2d_1 - d_2) + \frac{w_2^2}{6} \right)_x \\ = rR(1 - r)p_x,\end{aligned}\quad (36)$$

and

$$\begin{aligned}q'(t) + (F_D(d_1, d_2, w_1, w_2, q) + F_H(d_1, d_2, R))_x \\ - \frac{rR}{9} (1 - 2d_1 - d_2) (1 + d_1 + 2d_2)_x \\ = -F_p(d_1, d_2, r, R)p_x,\end{aligned}\quad (37)$$

where

$$\begin{aligned}F_D(d_1, d_2, w_1, w_2, q) = \left( q^2 - \left( (1 - 2d_1 - d_2) \frac{w_1}{3} + (2 - d_1 - 2d_2) \frac{w_2}{3} \right)^2 \right) \\ + \left( \left( \frac{1 - 2d_1 - d_2}{3} \right) (w_1 + w_2)^2 + \left( \frac{1 + d_1 - d_2}{3} \right) w_2^2 \right),\end{aligned}$$

$$F_H(d_1, d_2, R) = \left( \frac{(1 - 2d_1 - d_2)^2 + R((1 + d_1 - d_2) + (1 - 2d_1 - d_2))^2}{18} \right)$$

and

$$F_p(d_1, d_2, r, R) = 3D(r, R) + rD(r, R)[(R(r - 1) - 2) + (2 + R(1 - 2r))d_1 + (1 + R(2 - r))d_2], \quad (38)$$

with

$$D(r, R) = \frac{[3 + r(R(r - 1) - 2)]^2}{3[1 + r(R(r - 1) - 1)]},$$

and where we have dropped the tildes for simplification. The set of equations (33) to (37) may now be rewritten as the *non-Boussinesq* system, given by equations (33), (34) and

$$\begin{aligned} w_{1,t} + qw_{1,x} &+ \left( \left( \frac{2d_1 + d_2}{3} \right) (1 - w_1^2) - \frac{w_1 w_2}{3} (1 + d_1 + 2d_2) - \frac{w_1^2}{6} \right)_x \\ &- \frac{rR}{3} \left( \frac{1 + d_1 + d_2}{3} \right)_x \\ &- \frac{r^2 R}{9} \left( \frac{(1 - 2d_1 - d_2)(1 + d_1 + 2d_2)_x}{F_p(d_1, d_2, r, R)} \right) \\ &+ r \left( \frac{(F_D(d_1, d_2, w_1, w_2, q) + F_H(d_1, d_2, R))_x}{F_p(d_1, d_2, r, R)} \right) \\ &= - \frac{rq'}{F_p(d_1, d_2, r, R)}, \end{aligned} \quad (39)$$

$$\begin{aligned} w_{2,t} + qw_{2,x} &+ \left( \left( \frac{d_1 + 2d_2}{3} \right) (R - w_2^2) + \frac{w_1 w_2}{3} (1 - 2d_1 - d_2) + \frac{w_2^2}{6} \right)_x \\ &+ rR(1 - r) \left( \frac{(F_D(d_1, d_2, w_1, w_2, q) + F_H(d_1, d_2, R))_x}{F_p(d_1, d_2, r, R)} \right) \\ &- \frac{r^2 R^2 (1 - r)}{9} \left( \frac{(1 - 2d_1 - d_2)(1 + d_1 + 2d_2)_x}{F_p(d_1, d_2, r, R)} \right) \\ &= - \frac{rR(1 - r)q'}{F_p(d_1, d_2, r, R)}. \end{aligned} \quad (40)$$

## 2.2. The Boussinesq equations

The Boussinesq limiting case, when the difference of densities are negligible, can be seen as a particular case of the equations above. First, note that in the limit  $r \rightarrow 0$ , Equation (38) becomes

$$F_p(d_1, d_2, r, R) = 9.$$

It follows that (32) can be written in conservation form

$$q'(t) + (F_D(d_1, d_2, w_1, w_2, q) + F_H(d_1, d_2, R) + 9p)_x = 0,$$

and that the flux is a global conserved quantity depending on the boundary values of  $F_D - F_H + p$ . For example  $q' = 0$  in a periodic domain, in which case we can set  $q = 0$  by a Galilean transformation.

Thus, the three-layer shallow water Boussinesq equations in a periodic domain can be derived by setting  $q = 0$  and by taking the limit  $r \rightarrow 0$  in the non-Boussinesq equations (33), (34), (39) and (40). It follows that

$$\begin{aligned} d_{1,t} + \left( \frac{w_1}{3}(1 - d_2) - \frac{d_1}{3}(w_1 + w_2) \right)_x \\ - \left( \frac{d_1^2}{3}(2w_1 + w_2) + \frac{d_1 d_2}{3}(w_1 + 2w_2) \right)_x = 0, \end{aligned} \quad (41)$$

$$\begin{aligned} d_{2,t} + \left( \frac{w_2}{3}(1 + d_1) + \frac{d_2}{3}(w_1 + w_2) \right)_x \\ - \left( \frac{d_2^2}{3}(w_1 + 2w_2) + \frac{d_1 d_2}{3}(2w_1 + w_2) \right)_x = 0, \end{aligned} \quad (42)$$

$$w_{1,t} + \left( \left( \frac{2d_1 + d_2}{3} \right) (1 - w_1^2) - \frac{w_1^2}{6} - \left( \frac{1 + d_1 + 2d_2}{3} \right) w_1 w_2 \right)_x = 0, \quad (43)$$

$$w_{2,t} + \left( \left( \frac{d_1 + 2d_2}{3} \right) (R - w_2^2) + \frac{w_2^2}{6} + \left( \frac{1 - 2d_1 - d_2}{3} \right) w_1 w_2 \right)_x = 0. \quad (44)$$

We shall refer to this limit as the *Boussinesq limit* and the resulting equations as the *Boussinesq system*. We note that in the literature, however, the Boussinesq system is often reserved for weakly dispersive, weakly non-linear bidirectional shallow water waves. The rescaling and limit above is a mathematically formal way of deriving the Boussinesq system, instead of the physically based approach of ignoring density variations in the inertial terms, commonly used in the literature [4].

### 3. Results on three-layer flows

#### 3.1. Boundary conditions and the Benjamin paradox

The flux  $q$  and the deviation pressure  $p$  are related by Equation (37), which may result in the non-locality of the pressure, depending on the boundary conditions. As shown before, in the Boussinesq case, the volume

flux is constant (unless externally forced to be non-constant) and can be eliminated from the system.

*Sidewalls* or *no-flux* conditions force a behaviour similar to the non-Boussinesq case, as  $q = 0$  and Equation (37) becomes

$$p_x = -\frac{(F_D + F_H)_x}{F_p} + \frac{rR(1 - 2d_1 - d_2)(1 + d_1 + 2d_2)_x}{9F_p}. \quad (45)$$

It is possible then to insert (45) into equations (39) and (40) and close the system, eliminating the pressure.

For the case of *periodic* boundary conditions (of period  $L$ ), then we can remove the pressure from (37) and find a nonlocal evolution equation for the flux:

$$\begin{aligned} q' = & -\left(\int_{-L/2}^{L/2} (F_p)^{-1} dx\right)^{-1} \int_{-L/2}^{L/2} (F_p)^{-1} (F_H + F_D)_x dx \\ & + \frac{rR}{9} \left(\int_{-L/2}^{L/2} (F_p)^{-1} dx\right)^{-1} \int_{-L/2}^{L/2} (F_p)^{-1} (1 - 2d_1 - d_2)(1 + d_1 + 2d_2)_x dx. \end{aligned}$$

We can then replace  $q'$  above in (37) to compute the pressure, which can then be substituted in (39) and (40) to close the system which itself becomes nonlocal.

A related issue is the *Benjamin paradox* (Camassa *et al.* [16] and Benjamin [19]) which arises from the observation that stratified flows between two horizontal walls may not conserve horizontal momentum - a paradox as there is no apparent mechanism for a net horizontal force to be applied on the fluid.

Consider the case in which far-field conditions are imposed. There are two possibilities, either  $q$  is time-independent, and one can set  $q = q' = 0$  and the sidewall case is recovered, or, one may have even stronger far-field conditions imposed on the physical variables, such as  $h_j$  achieving the same constant value and  $u_j \rightarrow 0$  as  $x \rightarrow \pm\infty$ . Thus,  $q = 0$  and one can compute the difference of the values attained by the pressure at the far-field extremes, denoted by  $[p]_{-\infty}^{+\infty}$ , from Equation (37), yielding

$$\begin{aligned} [p]_{-\infty}^{+\infty} = & -\int_{-\infty}^{+\infty} (F_p)^{-1} (F_H + F_D)_x dx \\ & - \frac{rR}{9} \int_{-\infty}^{+\infty} (F_p)^{-1} (1 - 2d_1 - d_2)(1 + d_1 + 2d_2)_x dx. \end{aligned} \quad (46)$$

The total (horizontal) momentum is defined as the integral of the local horizontal momentum

$$M = \rho_1 h_1 u_1 + \rho_2 h_2 u_2 + \rho_3 h_3 u_3,$$

written above in the flow variables  $h_j$ ,  $u_j$ . Note that the momentum equations (25) to (27) implies that

$$M_t + \left( \sum_{j=1}^3 \rho_j h_j u_j^2 + (\rho_1 - \rho_3) \frac{h_1^2}{2} + (\rho_2 - \rho_3) \frac{h_2^2}{2} (\rho_1 - \rho_3) h_1 h_2 \right)_x = -P_x$$

and hence, rescaling the variables as in Section 2.1.5, integrating in  $x$  from  $-\infty$  to  $+\infty$  and using that  $u_j \rightarrow 0$  at infinity and that  $h_j$  tend to a same constant value when  $x \rightarrow \pm\infty$  lead to

$$\frac{d}{dt} \int_{-\infty}^{+\infty} M dx = -[p]_{-\infty}^{+\infty}.$$

Therefore, the total horizontal momentum is conserved if and only if the integrals on the right-hand side of (46) are zero, which is not the case for all choices of  $d_j$ ,  $w_j$ ,  $r$  and  $R$ .

This non-conservation arises from the fact that Equation (37) can be thought of as an elliptic problem for the pressure, and hence allowing the propagation of information about the flow at infinite speed to  $\pm\infty$ . This is not the case, for example, if the rigid lid is removed and replaced with either a free-surface or a flexible lid. Note that, for  $r \rightarrow 0$ , which corresponds to the Boussinesq approximation, the second integral disappears and denominator of the integrand  $F_p$  tends to a constant value, making the right-hand side a total derivative in  $x$  and therefore the conservation of momentum is recovered.

### 3.2. Linear waves on quiescent flows

Consider the general situation shown in Figure 1 and described by equations (1) to (11). By perturbing the uniform state of constant  $h_j \equiv H_j$  and zero  $u_j, v_j$ , with travelling wave modes proportional to  $e^{i(kx - \omega t)}$ , one obtains the following *dispersion relation* for  $\omega$ :

$$\begin{aligned} & [\rho_2 \cosh(|k|H_2)(\rho_3 \coth(|k|H_3) + \rho_1 \coth(|k|H_1)) \\ & + \sinh(|k|H_2)(\rho_2^2 + \rho_1 \coth(|k|H_1))\rho_3 \coth(|k|H_3)]\omega^4 \\ & + g|k|[\rho_2(\rho_3 - \rho_1) \cosh(|k|H_2) + \sinh(|k|H_2)((\rho_3 - \rho_2)\rho_1 \coth(|k|H_1) \\ & + (\rho_2 - \rho_1)\rho_3 \coth(|k|H_3))]\omega^2 \\ & + (g|k|)^2(\rho_3 - \rho_2)(\rho_1 - \rho_2) \sinh(|k|H_2)\omega = 0. \end{aligned}$$

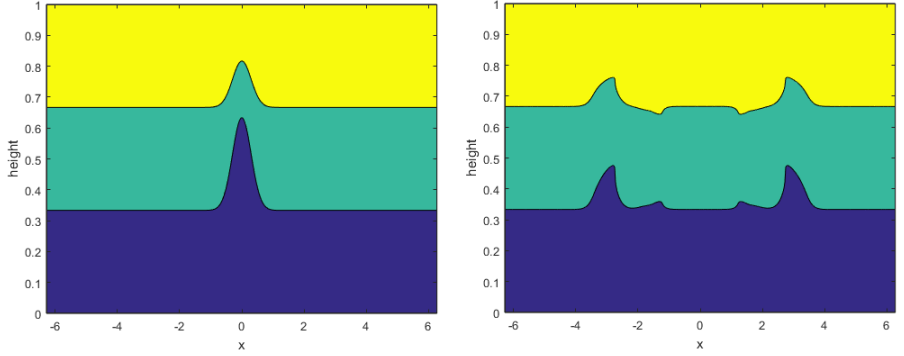


Figure 2: Evolution of a Gaussian pulse in a three-layer flow and its decomposition into mode 1 and mode 2 waves. The nonlinear equations (41) to (44) were solved to demonstrate both the splitting of pulses and the nonlinear steepening behind the mode 1 pulses.

Rescaling the variables as before and taking the shallow water limit, where  $|k|H_1, |k|H_2, |k|H_3 \ll 1$ , gives the equation for wave-speeds  $\lambda = \omega/k$  :

$$\begin{aligned}
 & (\rho_2\rho_3R_1 + \rho_1\rho_3R_2 + \rho_1\rho_2R_3) \lambda^4 \\
 & + ((\rho_2 - \rho_1)\rho_3R_1R_2 + (\rho_3 - \rho_1)\rho_2R_1R_3 + (\rho_3 - \rho_2)\rho_1R_2R_3) \lambda^2 \\
 & + (\rho_2 - \rho_1)(\rho_3 - \rho_2)R_1R_2R_3 = 0.
 \end{aligned}$$

Here,  $R_j = H_j/H$  with  $R_1/R_2, R_2/R_3$  of order 1. This biquadratic equation corresponds to two modes in each direction, one being the fast mode, usually called *mode 1* and the other being the slow mode, commonly referred as *mode 2*. These are numerically illustrated in Figure 2, where the evolution of a gaussian pulse decomposes into 4 smaller pulses (right panel), two of them travelling faster and with in-phase vertical displacements (mode 1 waves, seen at  $x \approx \pm 3$ ) and two moving slower and out-of-phase vertical displacements (mode 2 waves, seen at  $x \approx \pm 1.5$ ).

### 3.3. Symmetric solutions and evolutionary properties

In this section, we shall discuss the Boussinesq system, mainly in the special case where  $R = 1$  (*i.e.* the jumps in density are the same on both interfaces). Denoting the vector of solutions  $\mathbf{U} = (d_1, d_2, w_1, w_2)^T$ , the system may be written as

$$\mathbf{U}_t + A(\mathbf{U})\mathbf{U}_x = 0, \quad (47)$$

where  $A(\mathbf{U})$  is given from equations (41) to (44) by

$$-\frac{1}{3} \begin{pmatrix} w_1(1+4d_1+d_2) & w_1(1+d_1) & d_1(1+2d_1+d_2) & d_1(1+d_1+2d_2) \\ +w_2(1+2d_1+2d_2) & +w_2(2d_1) & +(d_2-1) & \\ \\ w_1(2d_2) & w_1(2d_1+2d_2-1) & d_2(2d_1+d_2-1) & d_2(d_1+2d_2-1) \\ +w_2(d_2-1) & +w_2(d_1+4d_2-1) & & -(d_1+1) \\ \\ 2(w_1^2-1) & (w_1^2-1) & w_1(1+4d_1+2d_2) & w_1(1+d_1+2d_2) \\ +w_1w_2 & +2w_1w_2 & +w_2(1+d_1+2d_2) & \\ \\ (w_2^2-R) & 2(w_2^2-R) & w_2(2d_1+d_2-1) & w_1(2d_1+d_2-1) \\ +2w_1w_2 & +w_1w_2 & & +w_2(2d_1+4d_2-1) \end{pmatrix}$$

For  $R = 1$ , these equations are invariant under the symmetry transformation

$$\begin{aligned} d_1 &\longleftrightarrow -d_2, \\ w_1 &\longleftrightarrow -w_2. \end{aligned}$$

More formally, for  $\mathbf{U} = (d_1, d_2, w_1, w_2)^T$ , there is an isomorphism  $\Phi$

$$\Phi(\mathbf{U}) = (-d_2, -d_1, -w_2, -w_1)^T.$$

and the system

$$\mathbf{U}_t + A(\mathbf{U})\mathbf{U}_x = 0 \tag{48}$$

is equivalent to

$$\tilde{\mathbf{U}}_t + A(\tilde{\mathbf{U}})\tilde{\mathbf{U}}_x = 0,$$

where  $\tilde{\mathbf{U}} \doteq \Phi(\mathbf{U})$ . Physically, this invariance corresponds to reversing the direction of gravity and exchanging the layers accordingly. For this reason, we shall refer to this configuration when  $R = 1$  as the *symmetric Boussinesq case*.

An immediate consequence is that the symmetric Boussinesq system allows pure mode 2 solutions. Suppose that

$$\begin{aligned} h_1(x, t) &= H(x, t), \\ h_2(x, t) &= h(x, t), \\ h_3(x, t) &= H(x, t), \end{aligned}$$

as illustrated in Figure 3. Then,

$$d_1 = h - H = -(H - h) = -d_2.$$

Define  $u_j$  in a similar fashion so that

$$w_1 = -w_2.$$

Writing

$$d \doteq d_1 \quad \text{and} \quad w \doteq w_1,$$

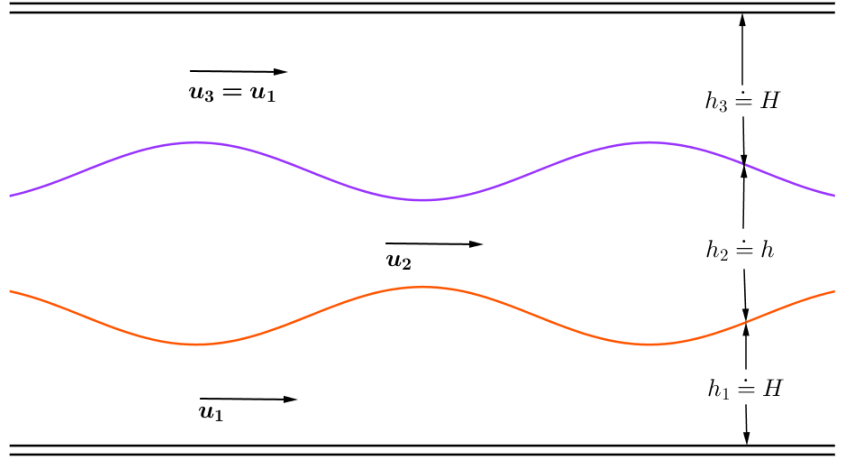


Figure 3: Illustration of a pure mode 2 solution in a three-layer flow.

the  $4 \times 4$  system of symmetric Boussinesq equations reduces to a pair of equations given by

$$\begin{aligned} d_t + \left( \frac{w}{3}(1 + d - 2d^2) \right)_x &= 0, \\ w_t + \left( \frac{d}{3}(1 - 2w^2) + \frac{w^2}{6} \right)_x &= 0. \end{aligned}$$

It is possible to show [20] that these pure mode 2 equations are equivalent to the two-layer shallow water ones [21]. This is physically evident in Figure 3 by imagining a boundary in the midline of the configuration. Consequently, this pure mode 2 dynamics is a two-dimensional invariant subspace of the four-dimensional system, and within that invariant subspace all prior results for the two-layer system applies. Most relevant is the result that the hyperbolic region in phase space  $(d, w) \in (-1/2, 1) \times (-1/\sqrt{2}, 1/\sqrt{2})$  (with  $w = w_1 = -w_2$ , and  $d = d_1 = -d_2$ ) is invariant under the evolution of the PDE. From a fluid dynamics perspective this means that for initial data satisfying this condition everywhere, the evolution remains wave-like and does not exhibit Kelvin-Helmholtz-like instabilities.

Motivated by these considerations, we propose describing the system using the variables

$$\begin{aligned} \bar{d} &= d_1 + d_2, & \tilde{d} &= d_2 - d_1, \\ \bar{w} &= w_1 + w_2, & \tilde{w} &= w_2 - w_1. \end{aligned}$$

Note that  $\bar{d} = 0$  and  $\bar{w} = 0$  are equivalent to the “pure” mode 2 case previously examined. Under this change of variables, the governing equations

can be rewritten as

$$\bar{d}_t + \left( \frac{\bar{w}}{6} (2 - 3\bar{d}^2) + \left( \frac{\bar{d}\tilde{w} + \tilde{d}\bar{w} - \bar{d}\tilde{d}\tilde{w}}{6} \right) \right)_x = 0, \quad (49)$$

$$\tilde{d}_t + \left( \frac{\tilde{w}}{6} (2 - \tilde{d}^2) - \left( \frac{\bar{d}\bar{w} + \tilde{d}\tilde{w} + 3\bar{d}\tilde{d}\tilde{w}}{6} \right) \right)_x = 0, \quad (50)$$

$$\bar{w}_t + \left( \frac{\bar{d}}{2} (2 - \bar{w}^2) + \frac{\bar{w}\tilde{w}}{6} (1 - \tilde{d}) \right)_x = 0, \quad (51)$$

$$\tilde{w}_t + \left( \frac{\tilde{d}}{6} (2 - \tilde{w}^2) + \left( \frac{\bar{w}^2}{4} - \frac{\tilde{w}^2}{12} - \frac{\bar{d}\bar{w}\tilde{w}}{2} \right) \right)_x = 0. \quad (52)$$

which, in the form (47) with  $\mathbf{U} = (\bar{d}, \tilde{d}, \bar{w}, \tilde{w})^T$ , has  $A(\mathbf{U})$  given by

$$\frac{1}{6} \begin{pmatrix} \tilde{w} - \tilde{d}\tilde{w} - 6\bar{d}\bar{w} & \bar{w} - 6\tilde{d}\tilde{w} & 2 + \tilde{d} - 3\bar{d}^2 & \bar{d}(1 - \tilde{d}) \\ -\bar{w}(1 + \tilde{d}) & -(\tilde{w} + 2\tilde{d}\tilde{w} + 3\bar{d}\bar{w}) & -\tilde{d}(1 + \bar{d}) & 2 - \tilde{d} - \bar{d}^2 \\ 6 - 3\bar{w}^2 & -\bar{w}\tilde{w} & \tilde{w} - \tilde{d}\tilde{w} - 6\bar{d}\bar{w} & \bar{w}(1 - \tilde{d}) \\ -3\tilde{w}\bar{w} & 2 - \tilde{w}^2 & 3(\bar{w} - \bar{d}\tilde{w}) & -(\tilde{w} + 2\tilde{d}\tilde{w} + 3\bar{d}\bar{w}) \end{pmatrix}. \quad (53)$$

The phase space  $\mathbb{R}^4$  can be decomposed as a direct sum of  $B_1$  and  $B_2$ :

$$B_1 = \{\mathbf{U} = (\bar{d}, \tilde{d}, \bar{w}, \tilde{w})^T \text{ such that } \tilde{d} = \tilde{w} = 0\},$$

$$B_2 = \{\mathbf{U} = (\bar{d}, \tilde{d}, \bar{w}, \tilde{w})^T \text{ such that } \bar{d} = \bar{w} = 0\}.$$

We shall consider the evolution of periodic solutions in phase space, where they correspond to closed curves. This situation is schematically presented in Figure 4.

If the initial condition  $\bar{d}|_{t=0} = \bar{w}|_{t=0} = 0$  holds for all points in the domain, then, from (49) to (52),  $\bar{d} = \bar{w} = 0$  for all  $t > 0$  and the system reduces to a pair of equations, which are the two-layer shallow water Boussinesq equations previously mentioned. The solution is trapped in the invariant plane  $B_2$  as shown in Figure 4(a).

Suppose now that the initial data is tangent to  $B_2$  at a single point, say  $x = x^*$ , as shown in Figure 4(b). Thus  $\mathbf{U}_x|_{t=0, x=x^*}$ , which is the tangent vector to the solution curve is in  $B_2$  and therefore it can be shown from (53) that  $(A(\mathbf{U})\mathbf{U}_x)|_{t=0, x=x^*} = -\mathbf{U}_t|_{t=0, x=x^*}$  is also in this plane. Contrary to intuition, this is not enough to guarantee that the point of tangent contact will always remain in  $B_2$ . In fact the point of contact will lose tangency and then may escape from  $B_2$  given that  $B_2$  has co-dimension greater than one. (Such behaviour does not occur in  $2 \times 2$  systems where invariant subspaces are simple waves, and periodic solutions never lose tangency to a simple wave [12].) A direct consequence of

this is that periodic initial data that transverses  $B_2$  can also leave  $B_2$  as the wave evolves. This is shown schematically in Figure 4(c) and a numerical solution illustrating the loss of tangency is presented in Figure 5. The invariance of  $B_2$  is also broken in the non-Boussinesq case and in the asymmetric Boussinesq case as exemplified numerically in Figure 6. The non-Boussinesq solution remains close to  $B_2$  despite strong stratification, with density differences of 20% between layers.

Now, suppose that  $\tilde{d}|_{t=0} = \tilde{w}|_{t=0} = 0$ , so that  $\mathbf{U}|_{t=0}$  is in  $B_1$ . It follows from equations (50) and (52) that

$$\tilde{d}_t|_{t=0} = \frac{1}{6} (\overline{dw})_x \neq 0, \quad (54)$$

$$\tilde{w}_t|_{t=0} = -\frac{1}{4} (\overline{w^2})_x \neq 0, \quad (55)$$

which implies that, in general,  $\tilde{d}_t \neq 0$  and  $\tilde{w}_t \neq 0$  for  $t > 0$ . Equations (54) and (55) represent the mode 2 production of a mode 1 wave. Consequently, any solution that is initially in  $B_1$  will immediately leave this region, as shown in Figure 4 (d). Physically, this means that no matter the initial “rest” configuration, if pycnoclines are initially displaced equally the evolution will generate mode 2 waves. Of course, “pure” mode 1 waves can be constructed using simple waves as shown next.

### 3.4. Simple waves

For a system of PDEs of the form (47), *simple waves* [22] (sometimes called *rarefaction waves* [23]) are special solutions that can be written as

$$\mathbf{U}(x, t) \doteq \mathbf{V}(\theta(x, t)). \quad (56)$$

These are important because they correspond to the individual waves of the system. Replacing Equation (56) into (47) yields

$$\mathbf{V}_\theta \theta_t + A(\mathbf{V}) \mathbf{V}_\theta \theta_x = 0, \quad (57)$$

which has a solution only if  $A(\mathbf{V}) \mathbf{V}_\theta$  is proportional to  $\mathbf{V}_\theta$ , leading to the eigenvalue problem

$$[A(\mathbf{V}(\theta)) - \lambda(\theta)I] \mathbf{V}_\theta(\theta) = 0, \quad (58)$$

and where  $\theta(x, t)$  must obey the hyperbolic PDE (if the original system is hyperbolic)

$$\theta_t + \lambda(\theta)\theta_x = 0. \quad (59)$$

The eigenvectors  $\mathbf{V}_\theta$  from Equation (58) yield, for each eigenvalue family, a vector field in the phase space whose integral curves are the simple waves ( $\mathbf{V}_\theta$  is tangent to these curves). For regions in phase space where

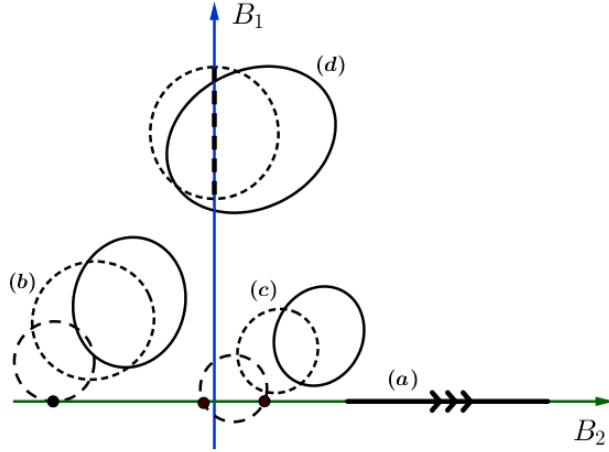


Figure 4: Decomposition of the four-dimensional phase space in the modal variables and schematic representation of a few solutions: in (c), it is shown that a given solution that initially touches the  $B_2$  might not intersect it anymore in future times. This happens even if the initial condition is tangent to  $B_2$  as in (b). On the other hand, if the initial condition is a pure mode 2, the solution will remain in mode 2 for all time (up to breaking) schematically shown in (a). The same does not happen for a initial condition lying in  $B_1$ . This set is not an invariant subspace and a general solution escapes as soon as it evolves on time, as seen in (d).

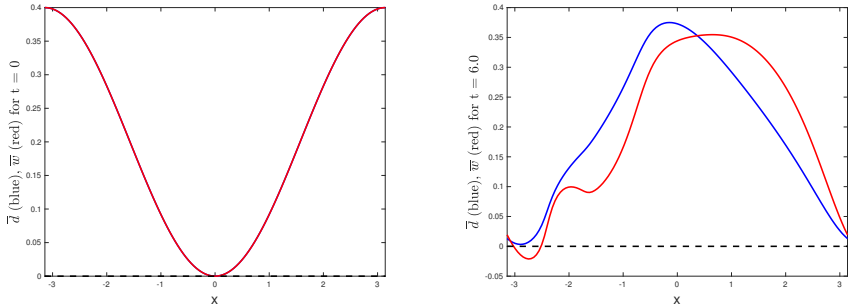


Figure 5: Numerical example of a solution which is initially tangent to the invariant plane  $B_1$ . Note that at  $t = 0$ , the solution satisfies  $\bar{d}(x_0) = \bar{w}'(x_0) = 0$  for  $x_0 = 0$  and therefore this is a point of tangency. At  $t = 6$ , this condition is no longer satisfied for any  $x_0$  in the domain.

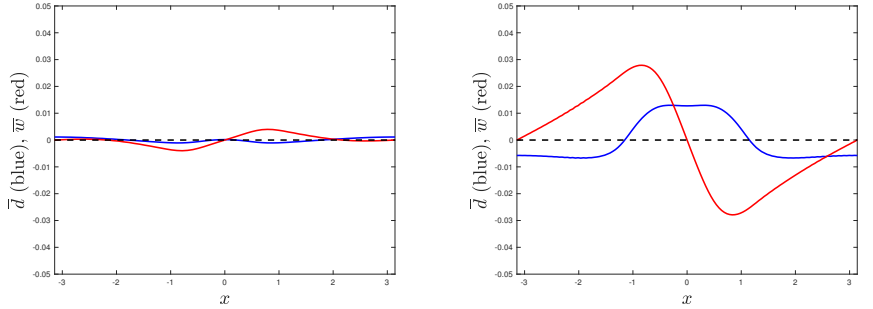


Figure 6: Numerical examples of how two different models break the invariant plane  $B_1$ . Left: A solution initially confined to the invariant plane  $B_1$  at  $t = 0$  evolving under the non-Boussinesq model (33)–(36) with  $r = 0.2$ ,  $R = 1.0$  and leaving the plane (i.e.  $\bar{d} \neq 0, \bar{w} \neq 0$ ). Right: A solution to the Boussinesq system with unequal stratification ( $R = 1.2$ ), initially confined to the invariant plane  $B_1$  at  $t = 0$  but evolving to leave the plane. All solutions shown at  $t = 3$ .

our system is strictly hyperbolic, this implies the existence of 4 curves through each point. Each of these curves is a simple wave and is invariant under the evolution of the PDE: solutions starting on these curves remain on them, only the parametrisation  $\theta(x, t)$  changes with time. Thus the 4 eigenvectors at each point yield a local basis of the phase space providing a decomposition based on in terms of the wave speeds  $\lambda$ , or, physically speaking, in terms of the two (fast) mode 1 waves and the two (slow) mode 2 waves. Examples of numerically computed evolution of simple waves in the physical system are shown in Figures 7, 8 and 9. Figures 8 and 9 also highlight the effectiveness of the modal decomposition in approximating the different families.

We remark also that the systems have a “left-right” symmetry evident in phase space. Given a simple wave through a point  $\mathbf{U} = (d_1, d_2, w_1, w_2)^T$  at which the characteristic speed is  $\lambda$ , there is a corresponding “reflected” simple wave through the point  $\tilde{\mathbf{U}} = (d_1, d_2, -w_1, -w_2)^T$  with characteristic speed  $-\lambda$ , i.e. propagating in the other direction. This is physically intuitive and can be seen explicitly by the structure of  $A(\mathbf{U})$ .

Simple waves are of crucial importance in the study of nonlinear first order hyperbolic PDEs. In two-dimensional systems, they define invariant regions [24], [12] due to the property that simple waves do not allow a general solution to cross it tangentially [25]. Furthermore, for mixed-type first order PDE systems, if an initial condition can be bounded by simple waves that do not themselves reach the boundary of the hyperbolic region, then the solution will remain hyperbolic until breaking. Therefore, using

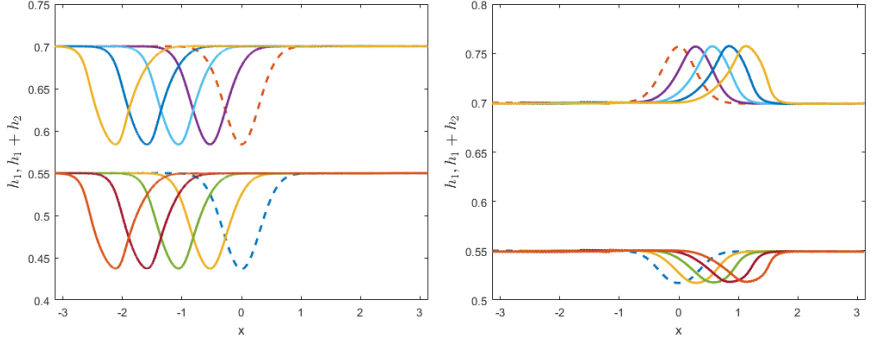


Figure 7: The evolution of the interfaces for a mode 1 (left) and mode 2 (right) simple wave solutions to the Boussinesq equations (41)-(44). The vertical extent of the channel is  $[0, 1]$ . The dashed line is the initial data and the solution is shown at various times. Note the nonlinear steepening of the wave.

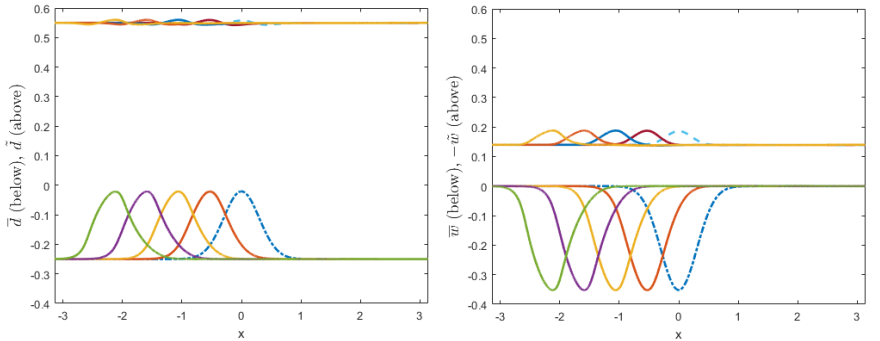


Figure 8: Evolution of the mode 1 simple wave solution shown in Figure 7, now in the modal variables of (49) to (52). Note the relatively small  $\tilde{d}$  and  $\tilde{w}$  components.

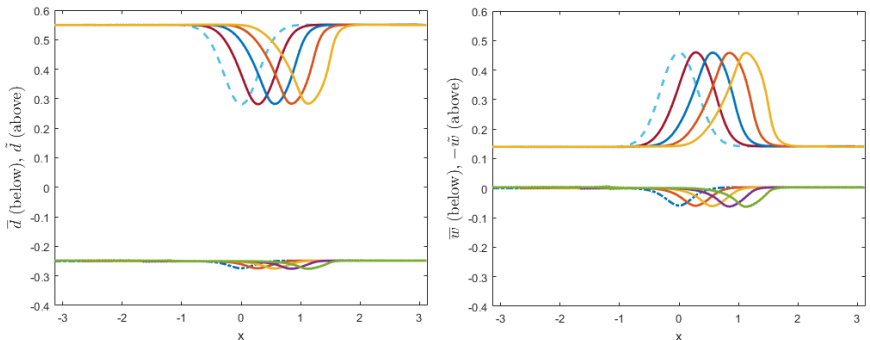


Figure 9: Evolution of the mode 2 simple wave solution shown in Figure 7, now in the modal variables of (49) to (52). Note the relatively small  $\bar{d}$  and  $\bar{w}$  components.

simple waves one can build the largest such region, which can be seen as a sharp bound to on hyperbolic initial data that prevents the solution straying into the elliptic region and therefore rendering the problem ill-posed [12]. Figure 10 illustrates the use of simple waves. It shows the evolution of a periodic initial condition in the invariant plane  $\bar{d} = \bar{w} = 0$ , and bounding simple waves.

In systems larger than two-dimensions, simple waves still provide a construction of “pure” wave solutions, but are less useful for bounding solutions, except in particular cases, for example when there is an invariant subspace as discussed above and showed in Figure 10.

Our first question is to explore whether there are other two-dimensional subspaces for mode 1 or mode 2 waves. These manifolds would contain families of both simple waves that exist for each mode of motion and would allow one to construct initial data that has waves propagating in both directions in a single mode of the system.

Such manifolds do not exist for general systems. The reason is due to the non-existence of an integrating factor for general differential forms in dimensions greater than two and, which implies that Riemann invariants, which would allow us to construct such manifolds, do not exist generically [26].

In general, a  $n$ -dimensional system of PDEs of the form (47) can be associated with up to  $n$  Riemann invariants. The  $j^{\text{th}}$  Riemann invariant is a smooth function  $R_j$  associated to the  $j^{\text{th}}$  eigenvalue, and satisfying

$$\nabla R_j = \mu \mathbf{w}_j,$$

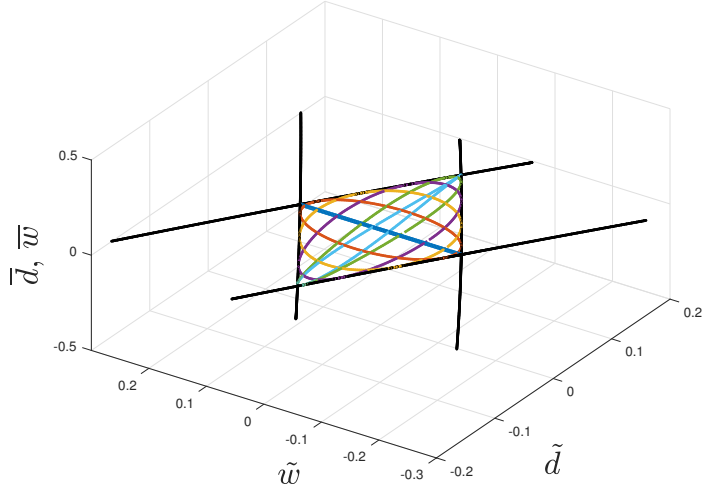


Figure 10: Evolution of a solution of (49) to (52) starting in the invariant mode 2 plane, trapped by four bounding simple waves (in black). The initial condition is given by the blue straight line joining two edges of the quadrilateral, and the coloured curves are the solutions at different times.

where  $\mu$  is a function (the integrating factor) and  $\mathbf{w}_j$  is the  $j^{\text{th}}$  left eigenvector of the system,

$$\mathbf{w}_j^T A(\mathbf{U}) = \mathbf{w}_j^T \lambda_j.$$

In our case, all of these are functions of  $\mathbf{U} = (\bar{d}, \tilde{d}, \bar{w}, \tilde{w})^T$ .

Since the gradient of the  $j^{\text{th}}$  Riemann invariant is parallel to the  $j^{\text{th}}$  left eigenvector, it follows that the  $k^{\text{th}}$  right eigenvector  $\mathbf{v}_k$  is tangent to the surface defined by constant  $R_j$  if  $j \neq k$ , because  $\mathbf{w}_j \cdot \mathbf{v}_k = \delta_{j,k}$ . Furthermore, if  $\mathbf{U}_k(\theta)$  is an integral curve of  $\mathbf{v}_k$  (i.e. a simple wave), then the  $j^{\text{th}}$  Riemann hypersurface contains this curve since

$$\frac{d}{d\theta} R_j(\mathbf{U}_k(\theta)) = \nabla R_j \cdot \mathbf{v}_k = 0.$$

Thus, in general, the hypersurface defined by  $R_j = \text{constant}$  contains  $n-1$  linearly independent simple waves associated to the  $n-1$  right eigenvalues of the system,  $\lambda_k$  for  $k \neq j$ .

Hence, if one wishes a family of, say, mode 2 simple waves to form a two-dimensional manifold in a four-dimensional phase space, it is necessary and sufficient that there be Riemann invariants associated to the

other two eigenvalues. The intersection of the surfaces defined by these two Riemann invariants then defines the manifold.

We have numerically attempted to construct such surfaces. This involves choosing a point in phase space and computing the two simple wave curves from a particular family (mode 1 or mode 2) that go through that point. These are the “spines” of an attempt to construct a mesh of simple waves: along each of these spines at regular intervals we construct new simple waves transversal to the spine. If the resulting mesh lies on a surface - i.e. all the simple waves intersect - we have evidence of an invariant subspace for the problem. As shown in Figures 11 and 12, families of simple waves for either mode 1 or mode 2 in the symmetric Boussinesq system do not intersect each other and therefore do not form a surface. Nevertheless the remarkable proximity to a surface can motivate different approximations that reduce the system.

### 3.5. Two-dimensional reduced models

Although the modal decomposition does not hold in general, Figures 8 and 9 suggest that an approximate decomposition might work well for the system. For mode 1 waves, notice that  $\tilde{d} \approx \text{constant}$  and that  $\tilde{w}$  varies slightly through the whole evolution of the wave. Therefore their dynamics could be simplified. We propose to set  $\tilde{d} \doteq \tilde{d}_0 \equiv \text{constant}$ , and solve Equation (50) to obtain  $\tilde{w} = f(\tilde{d}, \bar{w}; \tilde{d}_0)$  and hence get a two-dimensional system for  $\bar{d}$  and  $\bar{w}$  by replacing the expression for  $\tilde{w}$  in equations (49) and (51). The results of this approach are shown by Figures 13 to 16. In this particular example, we choose a Gaussian initial condition satisfying  $\tilde{d}(x, 0) = 0$  and  $\tilde{w}(x, t) = 0$  so that the solution lies in the hypothetical mode 1 plane defined by  $B_1$ . Note that there is a very good agreement between the full solution (plotted in solid blue) and the one given by the approximate 2 dimensional reduced model (plotted in dashed red lines). Figures 13 and 14 show the evolution of the mode 1 wave (as computed by the equations (49) and (51) whereas Figure 15 shows the error arising from assuming a constant  $\tilde{d}$  and Figure 16 shows the post-computed  $\tilde{w}$ . Since  $\tilde{w} = f(\tilde{d}, \bar{w}; \tilde{d}_0)$ , the approximation qualitatively captures the mode 1 (fast) component of  $\tilde{w}$  but fails to capture its mode 2 (slower) component.

In Figures 17 to 20, a similar reduction is attempted for a mode 2 wave, and the agreement between both models is even better. For these, we choose an initial condition satisfying  $\bar{d}(x, 0) = -0.15$  and  $\bar{w}(x, 0) = 0$  so that it lies in a plane parallel to the invariant plane  $B_2$ . In this case, we reduced the system by considering  $\bar{d} = \bar{d}_0 = -0.15$  and  $\bar{w} = f(\bar{d}, \tilde{w}; \bar{d}_0)$  as given by Equation (49). Figures 17 and 18 show the evolution of the mode 2 wave (as computed by the equations (50) and (52) whereas

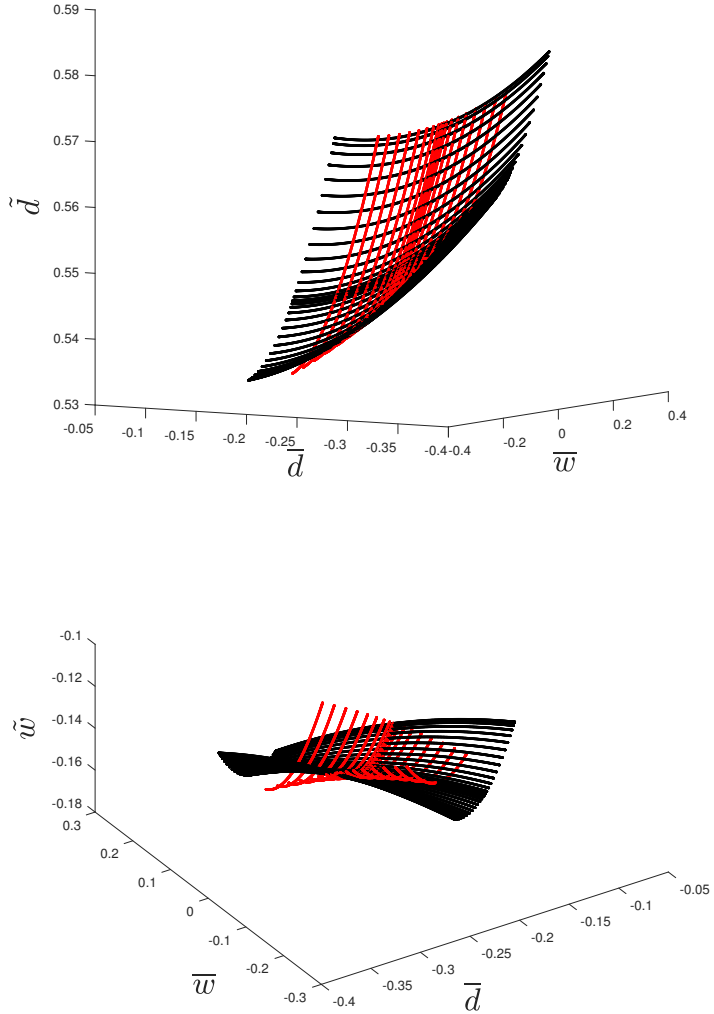


Figure 11: Families of mode 1 simple waves for the symmetric Boussinesq system (53). The two colours correspond to the two eigenvalues. Top: the projection onto  $\tilde{w} = 0$  shows that the curves almost lie on a surface. Bottom: For the projection onto  $\tilde{d} = 0$ , there is a clear non-intersection of simple waves.

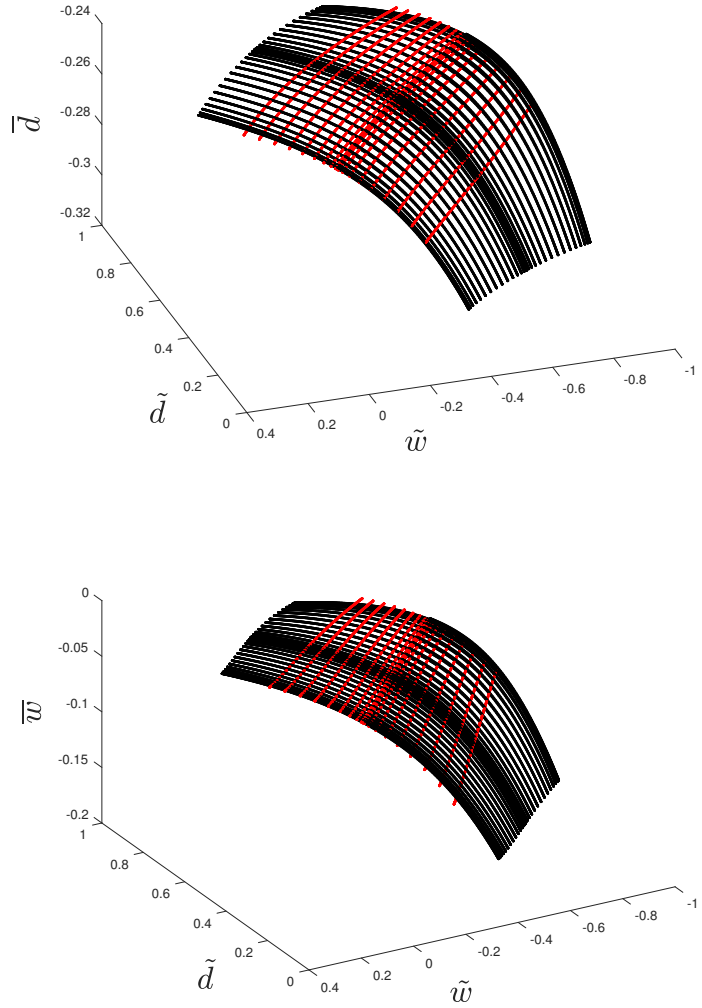


Figure 12: Families of mode 2 simple waves for the symmetric Boussinesq system (53). Both top and bottom figures show that, although the agreement is surprisingly good, these families do not form a surface.

Figure 19 shows the error arising from assuming a constant  $\bar{d}$  and Figure 20 shows the post-computed  $\bar{w}$ . Since  $\bar{w} = f(\bar{d}, \bar{w}; \bar{d}_0)$ , the approximation qualitatively captures the mode 2 (slow) component of  $\bar{w}$  but, as expected, fails to capture its faster mode 1 component.

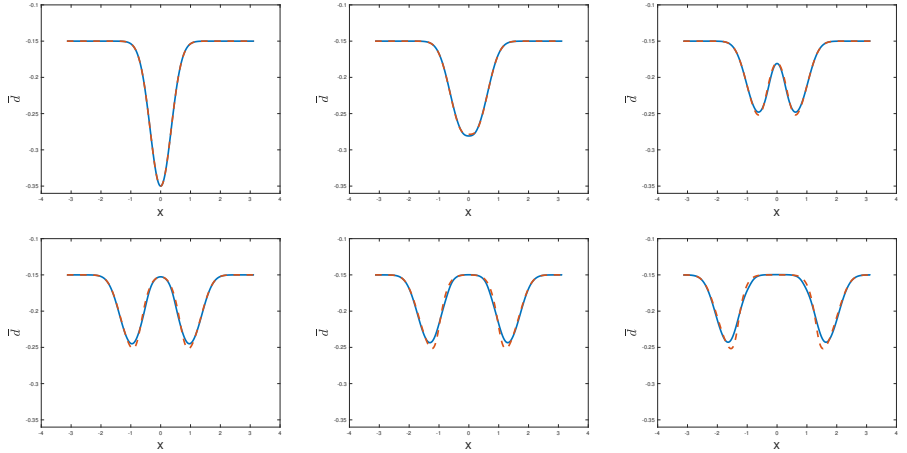


Figure 13: Solution of a reduced model for mode 1 waves (dashed line) compared to the solution of the full system (49) to (52) (solid line). From top left to bottom right,  $\bar{d}$  is plotted for  $t = 0, 0.6, 1.2, 1.8, 2.4$  and  $3.0$ .

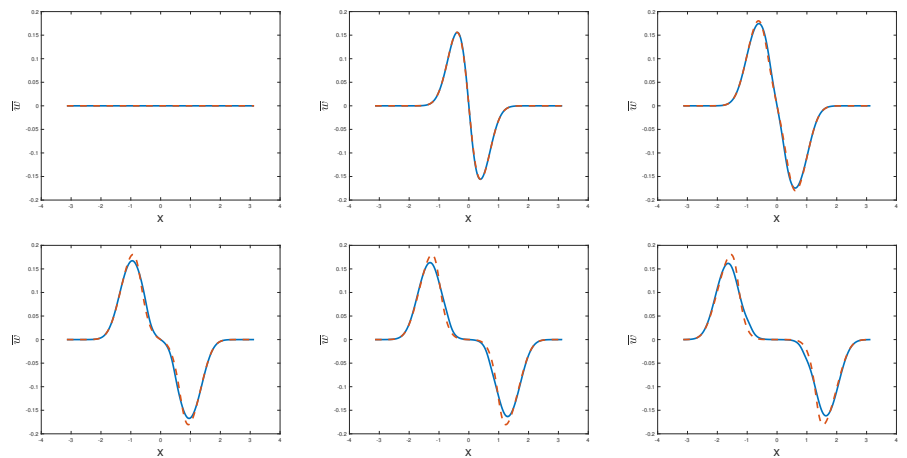


Figure 14: Solution of a reduced model for mode 1 waves (dashed line) compared to the solution of the full system (49) to (52) (solid line). From top left to bottom right,  $\bar{w}$  is plotted for  $t = 0, 0.6, 1.2, 1.8, 2.4$  and  $3.0$ .

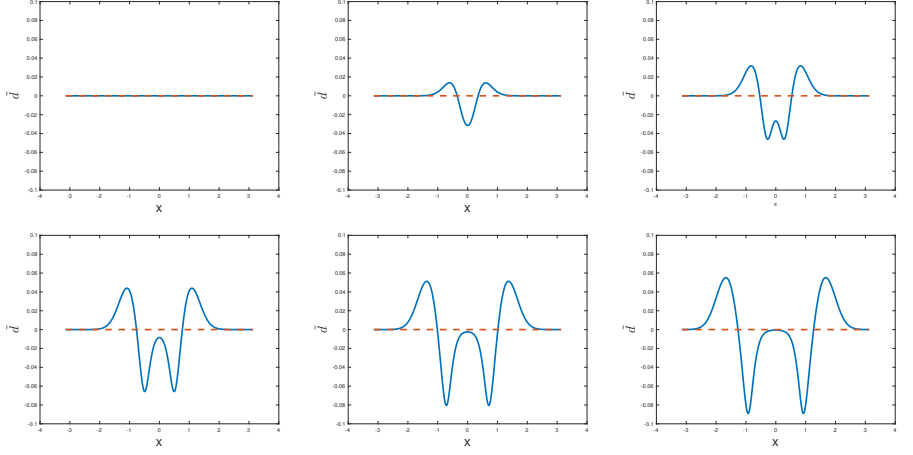


Figure 15: Solution of a reduced model for mode 1 waves (dashed line) compared to the solution of the full system (49) to (52) (solid line). From top left to bottom right,  $\tilde{d}$  is plotted for  $t = 0, 0.6, 1.2, 1.8, 2.4$  and  $3.0$ .

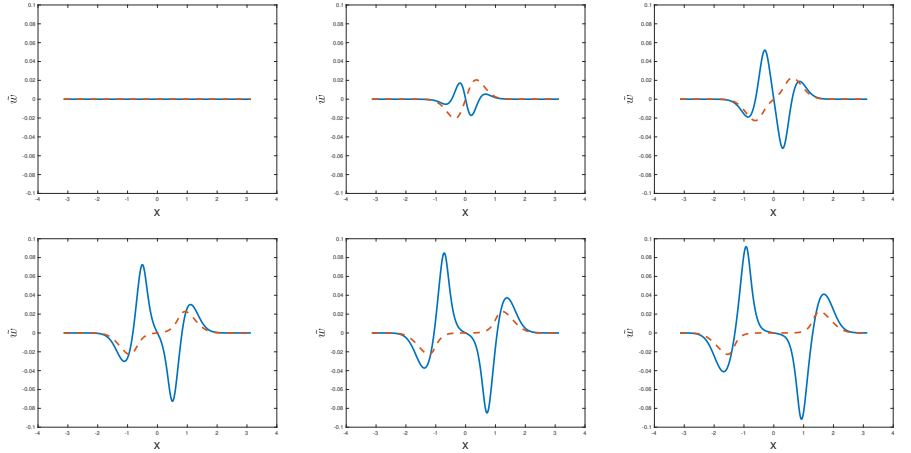


Figure 16: Solution of a reduced model for mode 1 waves (dashed line) compared to the solution of the full system (49) to (52) (solid line). From top left to bottom right,  $\tilde{w}$  is plotted for  $t = 0, 0.6, 1.2, 1.8, 2.4$  and  $3.0$ .

#### 4. Conclusions

We have derived the equations for long waves in a three-layer channel and explored some of their properties, both in the Boussinesq and in the general case. In the Boussinesq case, when the density jumps between layers is equal, a simple change of variables aids in separating the mode 1 and

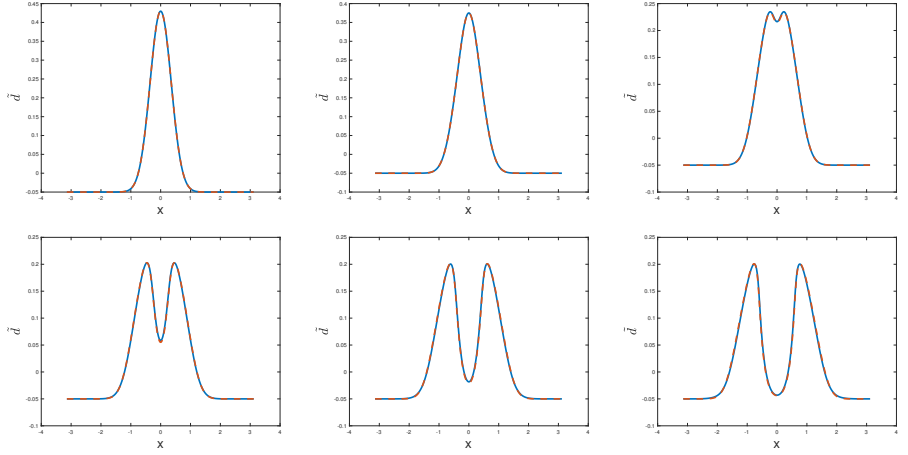


Figure 17: Solution of a reduced model for mode 2 waves (dashed line) compared to the solution of the full system (49) to (52) (solid line). From top left to bottom right,  $\tilde{d}$  is plotted for  $t = 0, 0.6, 1.2, 1.8, 2.4$  and  $3.0$ .

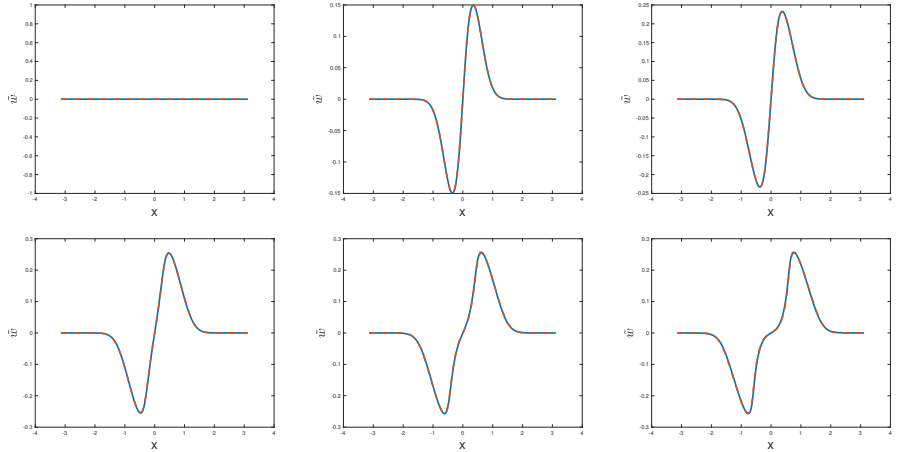


Figure 18: Solution of a reduced model for mode 2 waves (dashed line) compared to the solution of the full system (49) to (52) (solid line). From top left to bottom right,  $\tilde{w}$  is plotted for  $t = 0, 0.6, 1.2, 1.8, 2.4$  and  $3.0$ .

mode 2 dynamics. We then make use of simple waves in the Boussinesq case to test whether lower dimensional solution spaces can be constructed. We find that such invariant subspaces cannot be constructed, but that some ad-hoc reductions motivated by the computations are successful at capturing much of the features of the solution more accurately for mode 2 waves. These ideas provide a framework for creating reduced models

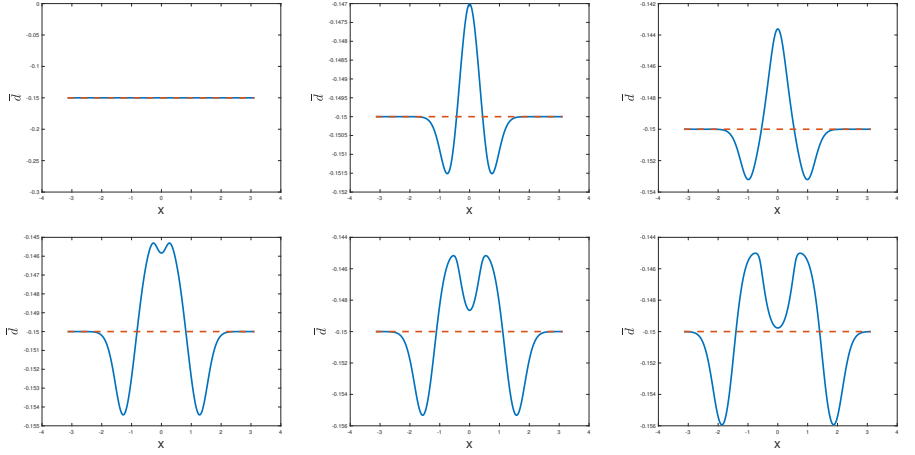


Figure 19: Solution of a reduced model for mode 2 waves (dashed line) compared to the solution of the full system (49) to (52) (solid line). From top left to bottom right,  $\bar{d}$  is plotted for  $t = 0, 0.6, 1.2, 1.8, 2.4$  and  $3.0$ .

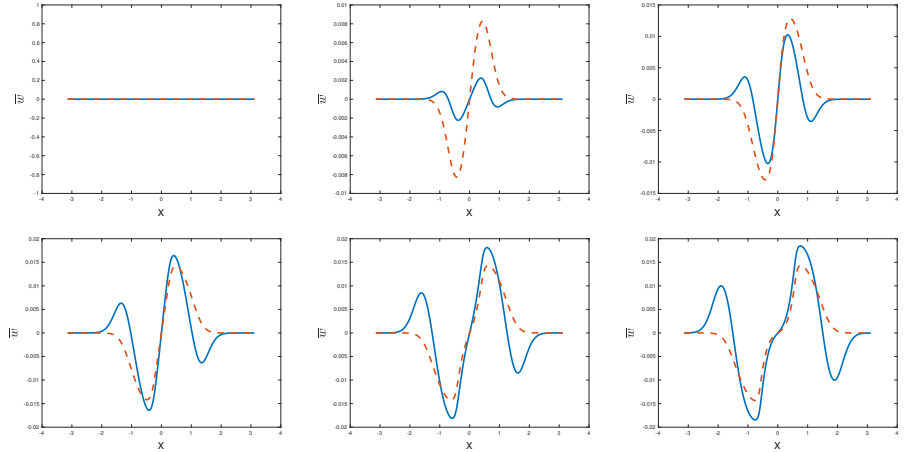


Figure 20: Solution of a reduced model for mode 2 waves (dashed line) compared to the solution of the full system (49) to (52) (solid line). From top left to bottom right,  $\bar{w}$  is plotted for  $t = 0, 0.6, 1.2, 1.8, 2.4$  and  $3.0$ .

which warrant further exploration. The Boussinesq approximation simplifies the system considerably and allows for symmetries to be exploited while retaining accuracy. A full numerical study of the non-Boussinesq equations is of interest, but outside the scope of this paper.

All solutions that we compute break after some time, and an interesting question is the inclusion of shocks in the dynamics and the required

Rankine-Hugoniot shock conditions. For two-layer flows this is a subject that still is an active area of research ([27], [28]). In particular each layer's momentum is not conserved but interfacial circulation is ([14],[28]) and one can also ask whether there is a choice of shock conditions which can allow for a realistic model of entrainment between the layers ([29], [14]). Generally speaking, there has been little or no study of shocks in the multi-layer case.

### Acknowledgments

The work of F.d.M.V. was supported by CNPq - Conselho Nacional de Desenvolvimento Científico e Tecnológico (Brasil) under the grant number 249770/2013-0, to whom both researchers are grateful.

### References

1. T. P. STANTON and L. OSTROVSKY, Observations of highly nonlinear internal solitons over the continental shelf, *Geophys. Res. Lett.* 25:2695–2698 (1998).
2. D. CHRISTIE and R. WHITE, The morning glory of the Gulf of Carpentaria, *Aust. Meteorol. Mag* 41:21–60 (1992).
3. K. R. HELFRICH and W. K. MELVILLE, Long nonlinear internal waves, *Annu. Rev. Fluid Mech.* 38:395–425 (2006).
4. B. CUSHMAN-ROISIN and J.-M. BECKERS, *Introduction to Geophysical Fluid Dynamics - Physical and Numerical Aspects*, 2nd ed., Academic Press, Waltham, 2011.
5. R. LONG, Long waves in a two-fluid system, *J. Meteorol.* 13:70–74 (1956).
6. D. J. BENNEY, Long non-linear waves in fluid flows, *Journal of Mathematics and Physics* 45:52–63 (1966).
7. R. GRIMSHAW, E. PELINOVSKY, and T. TALIPOVA, The modified Korteweg-de Vries equation in the theory of large-amplitude internal waves, *Nonlinear Processes in Geophysics* 4:237–250 (1997).
8. M. MIYATA, Long internal waves of large amplitude, *Nonlinear water waves*, Springer, 1988, pp. 399–406.
9. W. CHOI and R. CAMASSA, Fully nonlinear internal waves in a two-fluid system, *Journal of Fluid Mechanics* 396:1–36 (1999).
10. Y. J. YANG, Y. C. FANG, M.-H. CHANG, S. R. RAMP, C.-C. KAO, and T. Y. TANG, Observations of second baroclinic mode internal solitary waves on the continental slope of the northern South China Sea, *Journal of Geophysical Research: Oceans* 114 (2009), no. C10.
11. L. OVSYANNIKOV, Two-layer “shallow water” model, *Journal of Applied Mechanics and Technical Physics* 20:127–135 (1979).
12. A. BOONKASAME and P. A. MILEWSKI, The stability of large-amplitude shallow interfacial non-Boussinesq flows, *Stud. in Appl. Math.* 128:40–58 (2011).
13. R. ROTUNNO, J. B. KLEMP, G. H. BRYAN, and D. J. MURAKI, Models of non-Boussinesq lock exchange flow, *J. Fluid Mech.* 675:1–26 (2011).

14. P. A. MILEWSKI and E. G. TABAK, Conservation law modelling of entrainment in layered hydrostatic flows, *J. Fluid Mech.* 772:272–294 (2015).
15. T.-C. JO and Y.-K. CHOI, Dynamics of strongly nonlinear internal long waves in a three-layer fluid system, *Ocean Sci. J.* 49:357–366 (2014).
16. R. CAMASSA, S. CHEN, G. FALQUI, G. ORTENZI, and M. PEDRONI, An inertia ‘paradox’ for incompressible stratified Euler fluids, *J. Fluid Mech.* 695:330–340 (2012).
17. P. G. BAINES, *Topographic Effects in Stratified Flows*, 1st ed., Cambridge University Press, Cambridge, 1995.
18. R. S. JOHNSON, *A Modern Introduction to the Mathematical Theory of Water Waves*, 1st ed., Cambridge University Press, Cambridge, 1997.
19. T. B. BENJAMIN, On the Boussinesq model for two-dimensional wave motions in heterogeneous fluids, *J. Fluid Mech.* 165:445–474 (1986).
20. F. DE MELO VIRÍSSIMO, *Dynamical System Methods for Waves in Fluids: Stability, Breaking and Mixing*, Ph.D. thesis Department of Mathematical Sciences, University of Bath, United Kingdom (2018).
21. P. A. MILEWSKI, E. G. TABAK, C. V. TURNER, R. R. ROSALES, and F. A. MENZAQUE, Nonlinear stability of two-layer flows, *Comm. Math. Sci.* 2:427–442 (2004).
22. P. LAX, *Hyperbolic Systems of Conservation Laws and the Mathematical Theory of Shock Waves*, 1st ed., CBMS-NSF Regional Conference Series in Applied Mathematics, 1973.
23. A. A. MAILYBAEV and D. MARCHESIN, Hyperbolicity singularities in Rarefaction Waves, *J. Dynam. Differ. Eq.* 20:1–29 (2008).
24. L. CHUMAKOVA, F. A. MENZAQUE, P. A. MILEWSKI, R. R. ROSALES, and E. G. TABAK, Shear instability for stratified hydrostatic flows, *Comm. on Pure and Applied Math* 62:183–197 (2009).
25. L. CHUMAKOVA and E. G. TABAK, Simple waves do not avoid eigenvalue crossings, *Comm. on Pure and Applied Math* 63:119–132 (2010).
26. G. B. WHITHAM, *Linear and Nonlinear Waves*, 1st ed., Wiley-Interscience, 1974.
27. M. UNGARISH, A non-dissipative solution of Benjamin-type gravity current for a wide range of depth ratios, *Journal of Fluid Mechanics* 682:54–65 (2011).
28. Z. BORDEN and E. MEIBURG, Circulation-based models for Boussinesq internal bores, *Journal of Fluid Mechanics* 726 (2013).
29. P. A. MILEWSKI, T. JACOBSEN, and E. G. TABAK, Mixing closures for conservation laws in stratified flows, *Stud. in Appl. Math.* 121:89–116 (2008).

DEPARTMENT OF MATHEMATICAL SCIENCES, UNIVERSITY OF BATH, BATH, UNITED KINGDOM, BA2 7AY